Articles

Cathodic Properties of $LiCoO_2$ Synthesized by a Sol-Gel Method for Lithium Ion Battery

Pong-Jun Cho, Euh-Duck Jeong, and Yoon-Bo Shim*

Department of Chemistry, Pusan National University, Pusan 609-735, Korea
Recived July 29, 1997

$LiCoO_2$ powder was synthesized in an aqueous solution by a sol-gel method and used as a cathode active material for a lithium ion rechargeable battery. The layered $LiCoO_2$ powders were prepared by igniting in air for 12 hrs at 600 °C (600-$LiCoO_2$) and 850 °C (850-$LiCoO_2$). The structure of the $LiCoO_2$ powder was assigned to the space group R bar 3 m (lattice parameters a= 2.814 Å and c=14.04 Å). The SEM pictures of 600-$LiCoO_2$ revealed homogeneous and fine particles of about 1 μm in diameter. Cyclic voltammograms (CVs) of 600-$LiCoO_2$ electrode displayed a set of redox peaks at 3.80/4.05 V due to the intercalation/deintercalation of the lithium ions into/out of the $LiCoO_2$ structure. CVs for the 850-$LiCoO_2$ electrode had a major set of redox peaks at 3.88/4.13 V, and two small set of redox peaks at 4.18/4.42 V and 4.05/4.25 V due to phase transitions. The initial charge-discharge capacity was 156-132 mAh/g for the 600-$LiCoO_2$ electrode and 158-131 mAh/g for the 850-$LiCoO_2$ electrode at the current density of 0.2 mA/cm^2. The cycleability of the cell consisting of the 600-$LiCoO_2$ electrode was better than that of the 850-$LiCoO_2$. The diffusion coefficient of the Li^+ ion in the 600-$LiCoO_2$ electrode was calculated as 4.6×10^{-8} cm^2/sec.

Introduction

The lithium ion battery has received much attention due to its high operating voltages which lie in the 3.5-4.5 V range, in addition to its high energy density. This battery utilizes lithium host materials in which lithium ions intercalate and deintercalate into/from the anode and the cathode materials.[1]

The materials being examined as cathodes are the layered transition metal oxides, such as $LiCoO_2$,[2-7] $LiNiO_2$,[8,9] $LiCo_yNi_{1-y}O_2$,[10,11] and the oxides having a spinel structure, such as $LiMn_2O_4$.[12-14] Of these, $LiCoO_2$ has been examined widely and was commercialized for lithium ion batteries by Sony Energytec in 1991, although cobalt is more expensive and less intimate to environment than manganese oxides. The energy storage capacity of the commercialized lithium ion battery is ca. 100-125 Wh/kg (or 200-250 Wh/L). $LiCoO_2$ structure is based an a close-packed network of oxygen atoms with the Li^+ and Co^{3+} ions ordering on alternating (111) planes of the cubic rock salt structure. When the cell is charging, the lithium ions deintercalate from the $LiCoO_2$ structure. When the cell is discharging, the lithium ions intercalate into the Li_1-$XCoO_2$ structure. The reactions is as follows:

$$LiCoO_2 \underset{\text{discharge}}{\overset{\text{charge}}{\rightleftharpoons}} xLi^+ + Li_{1-x}CoO_2 + xe$$

In this reaction, the theoretical intercalation/deintercalation range of Li^+ ions through the $LiCoO_2$ frame is $0<x<1$, and the specific capacity is 274 mAh/g when x equals 1.0.

The preparation of an electrode material is important to achieve a good performance in the battery. Until recently, most researchers have prepared $LiCoO_2$ using solid phase reactions. However, solid phase reactions have disadvantages leading to the non-homogeneity of particles, abnormal grain growth, and poor control of stoichiometry. In order to improve these and to lower the synthesis temperature of compounds, solution phase preparation methods are better than solid phase reactions. There are a few reports which document the solution phase reaction methods of $LiCoO_2$, such as using a complex formation reaction with organic acids,[15,16] a sol-gel method,[18,19] and other precipitation reactions.[20] Until recentely, the several researchers reported about the preparation for $LiMn_2O_4$ in a solution.[18,21,22] We report herein the low temperature synthesis of the $LiCoO_2$ phase by means of a solution process. This solution teachnique is known as a sol-gel processing consists of the condensation of metal oxide networks from solution phase precusors. $LiCoO_2$ was synthesized through a sol-gel method with cobalt acetate in an alkaline solution at two different temperatures to improve its cycle life, and it was characterized as a cathode for the Lithium ion battery. To elucidate the characteristics of the $LiCoO_2$ powders prepared at two different temperatures, the chemical properties of the powders were investigated by thermal analysis, SEM, FT-IR spectroscopy, and X-ray diffractometry. In addition to the chemical properties, the electrochemical behaviors of the $LiCoO_2$ electrode were investigated employing cyclic voltammetry, charge/discharge experiments, and ac impedance spectroscopy. Additionally, the diffusivity of Li^+ ion in the electrode was evaluated from the impedance data.

*To whom correspondence should be addressed.

Experimental

Reagents and materials. An aqueous solution composed of $Co(OAc)_2 \cdot H_2O$ (Aldrich Co., 98+%, A.C.S. reagent), $LiOH \cdot H_2O$ (Aldrich Co.) and NH_4OH (Junsei Chemical Co., Ltd., Guaranted Reagent, 28%) was used to prepare the precursor of $LiCoO_2$ through hydrolysis. To prepare a $LiCoO_2$ cathode, $LiCoO_2$ powder, acetylene black as a conducting material, and *N*-methyl-2-pyrrolidinone (NMP) solution containing poly (vinylidene difluoride) (PVDF, Aldrich Co., average MW: 534,000) as a binder, were used. A stainless steel 316 ex-met (SUS-5/0; Mesh dimension, 0.05×0.03 in. Exmet Co.) was used as a current collector. A lithium foil compressed on a current collector was used as the counter and reference electrodes. The supporting electrolyte was a propylene carbonate (PC, Merck Co., battery grade) solution containing 1.0 M $LiClO_4$ (Aldrich Co.).

Synthesis of $LiCoO_2$. $LiCoO_2$ was synthesized by a sol-gel method, which was first reported by P. Barboux *et. al.*[18] An aqueous 3.0 M NH_4OH solution was added to 1.0 M LiOH solution. A 0.5 M aqueous $Co(OAc)_2$ solution was added to the mixed hydroxide solution while stirring. The reaction leads to gelatinous precipitates composed of dispersed particles of metal hydroxide. By evaporating the solvent in the gelatinous precipitates completely, the powdered precursor was obtained. Thermal gravimetric analyses (Dupont Co. analyzer) for $LiCoO_2$ powders and starting materials were performed in air at a heating rate of 10 °C/min. Based on the thermal data, heating temperatures of 600 and 850 °C were chosen. The $LiCoO_2$ powders were prepared at two temperatures as follows: For 600-$LiCoO_2$, the precursor powder was heat-treated at 600 °C for 36 hours followed by mixing and heating again at 600 °C for 24 hours. For 850-$LiCoO_2$, the precursor powder was heated at 600 °C for 12 hours, 850 °C for 24 hours and then heated again at 850 °C for 24 hours. Figure 1 displays the preparation diagram of the $LiCoO_2$ precursor and the electrode.

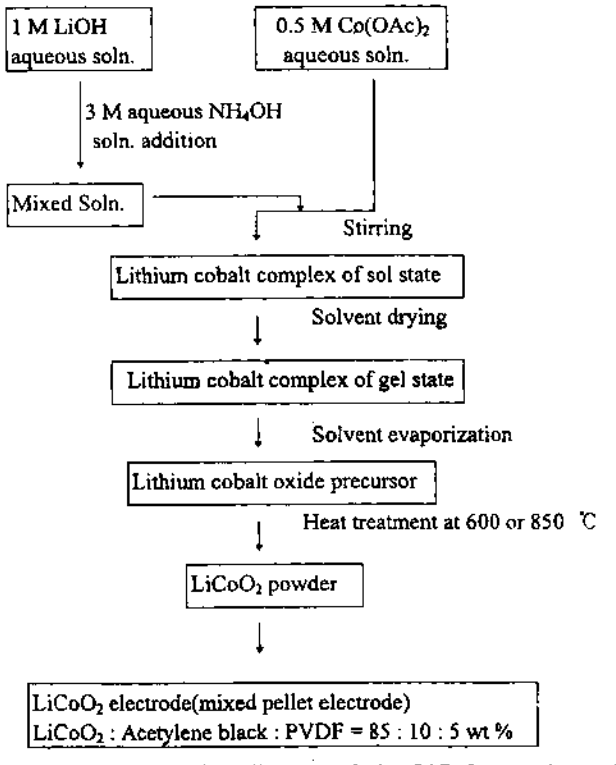

Figure 1. A preparation diagram of the $LiCoO_2$ powder and electrode.

Fabrication of electrodes. $LiCoO_2$ electrodes were prepared by adding a mix consisting of 85 wt% of $LiCoO_2$, 10 wt% of acetylene balck, and 5 wt% of PVDF to an NMP solution. The kneaded slurry in an adequate viscosity was coated on a stainless steel 316 ex-met with an apparent surface area of 1 cm^2. The prepared electrodes were dried at 100 °C in a vacuum oven for 24 hours, and then were used for the experiments.

Instrumentation. The $LiCoO_2$ powder was characterized by X-ray diffractometry (Rigaku X-ray diffractometer (D/Max)), IR spectroscopy (Bruker Co. Model 1FS 66), and scanning electron microscopy (Hitachi Co., S-2400). The electrochemical characteristics of $LiCoO_2$ electrodes were examined under an argon atmosphere in a glove box (JISCO Co., Korea). Cyclic voltammetry and chronopotentiometry were carried out employing Potentiostat/Galvanostat (PAR 273A and 363) with a Kipp & Zonen X-Y recorder. The impedance spectra were obtained by a PAR 273A coupled with a PAR 5210 lock-in amplifier.

Results and Discussion

Thermal and XRD patterns of $LiCoO_2$ powders. Optimum heat treatment temperatures for preparing the $LiCoO_2$ powders were determined with thermal analysis of the powders. The TG curve of the powder displayed two large deflections at the temperature ranges between 240 and 550 °C and between 600 and 780 °C (not shown).

While the weight losses at the first temperature range was about 20%, the losses at the second one was about 2%. Thus, we chose heat treatment temperatures of 600 and 850 °C. Figure 2 shows the XRD patterns for the $LiCoO_2$ powder treated at 600 and 850 °C. Little difference in the XRD patterns was observed between two heating temperature conditions. All diffraction peaks were indexed by assuming the structure to be a hexagonal lattice of the α-$NaFeO_2$ type. 600-$LiCoO_2$ has lattice parameters as follows: a-axis of 2.814 Å, c-axis of 14.04 Å, and c/a ratio of 4.989. These values are consistent with the previously reported values.[2] However, the XRD pattern of the 850-$LiCoO_2$ powder shows slightly different values as follows: a-axis of 2.742 Å, c-axis of 14.04 Å, and c/a ratio of 5.120. As shown in Figure 2(b), $LiCoO_2$ powders obtained with high temperature treatment exhibit higher (003) peak intensity than the powders obtained with lower temperature. This indicates that more order in the 850-$LiCoO_2$ is present in the atom arrangement compared to the powder synthesized at the low temperature.

To characterize the formation of the O-Co-O bond in the $LiCoO_2$ structure synthesized in the present work, we obtained FT-IR spectra of (a) the 600- and (b) 850-$LiCoO_2$ powders, and (c) a commercial $LiCoO_2$ powder supplied by Cyprus Foote Mineral Co. (CFM). The absorption peaks at 650, 600, and 530 cm^{-1} in the spectrum of the 600-$LiCoO_2$ powder are much stronger than those of CFM's and the 850-$LiCoO_2$ (Figure 3(b)). The bands of the $LiCoO_2$ powders

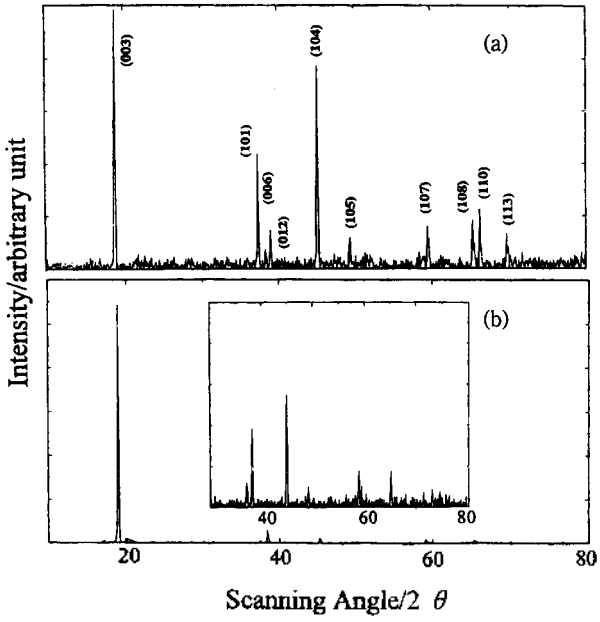

Figure 2. XRD patterns of the synthesized $LiCoO_2$ powders obtained by heating the precursor (a) at 600 °C and (b) at 850 °C. The miller indices are based on a hexagonal unit cell.

shifted toward high frequencies at 670, 633, and 540 cm^{-1} compared to those of CoO_4^{4-}, which arise from the O-Co-O vibration mode.[23] The high field shift of the absorption peaks seems to arise from the stronger interaction of the O-Co-O bond in $LiCoO_2$ than that of CoO_4^{4-}. The low intensity of the absorption peaks in the spectrum of 850-$LiCoO_2$ compared to that of 600-$LiCoO_2$ is expected due to the highly crystalline structure of $LiCoO_2$ prepared at the high temperature.

The surface morphologies of the $LiCoO_2$ powders were observed by the scanning electron microscopy as shown in Figure 4. The SEM obtained for the 600-$LiCoO_2$ powder (Figure 4(a)) shows homogeneous and fine particles of about 1 μm in size. The SEM of 850-$LiCoO_2$ powder shows an inhomogeneous and more widely distributed texture due to sintering by the high heating temperature (see Figure 4(b)).

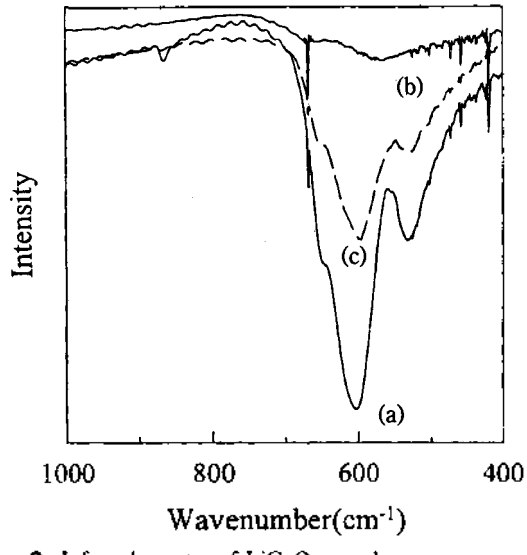

Figure 3. Infrared spectra of $LiCoO_2$ powders.

(a) heat-treated at 600℃

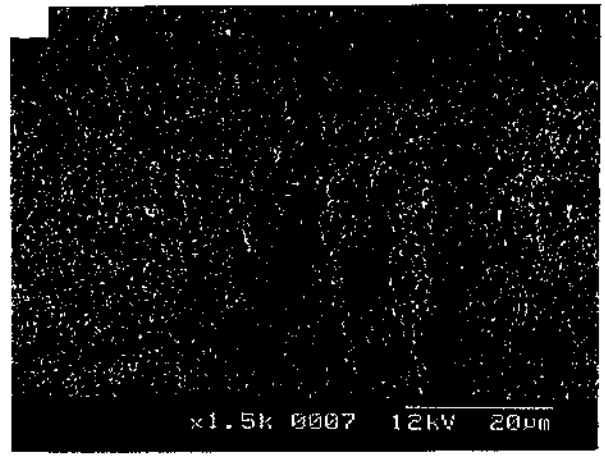

(b) heat-treated at 850℃.

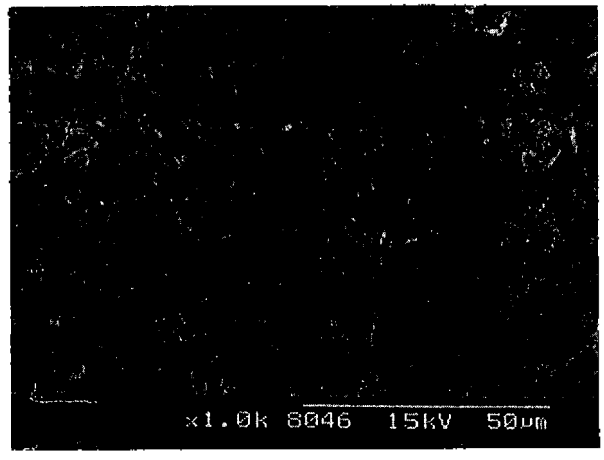

Figure 4. SEM pictures obtained for the 600- and 850-$LiCoO_2$ powders, respectively.

Cyclic voltammetric characteristics of $LiCoO_2$ electrodes. To examine the electrochemical properties of $LiCoO_2$ electrodes at an igniting temperature, cyclic voltammetry was conducted in 1 M $LiClO_4$/PC with a $LiCoO_2$ electrode. Figure 5 shows cyclic voltammograms (CVs) of both the 600- and 800-$LiCoO_2$ electrodes at a scan rate of 0.01 mV/sec and 1 mV/sec, respectively, in a potential range of 3.0 to 4.5 V. The open circuit voltage of a cell was about 3 V. A CV recorded for the 600-$LiCoO_2$ electrode shows a set of redox peaks at 3.80 and 4.05 V as shown in Figure 5(a). On the other hand, the CV for the 850-$LiCoO_2$ electrode shows one set of redox peaks at 3.88/4.13 V and two small sets of redox peaks at 4.18/4.42 V and 4.05/4.25 V (Figure 5(b)). The two redox peaks in the high potential range resulted from an ordered/disordered lithium ion arrangements in the crystal structure. This is similar to the results reported by Dahn *et al.*[4] In the cell with the 600-$LiCoO_2$ electrode, this type of phase transition did not appear. This implies that 600-$LiCoO_2$ may have a other structure compare to 850-$LiCoO_2$. Figure 5(c) and (d) show cyclic voltammograms recorded for the 600- and 850-$LiCoO_2$ electrodes at a scan rate of 1 mV/sec in a PC solution containing 1 M $LiClO_4$. In this scan rate, the redox peaks appeared irreversibly. The oxidation peak hardly ob-

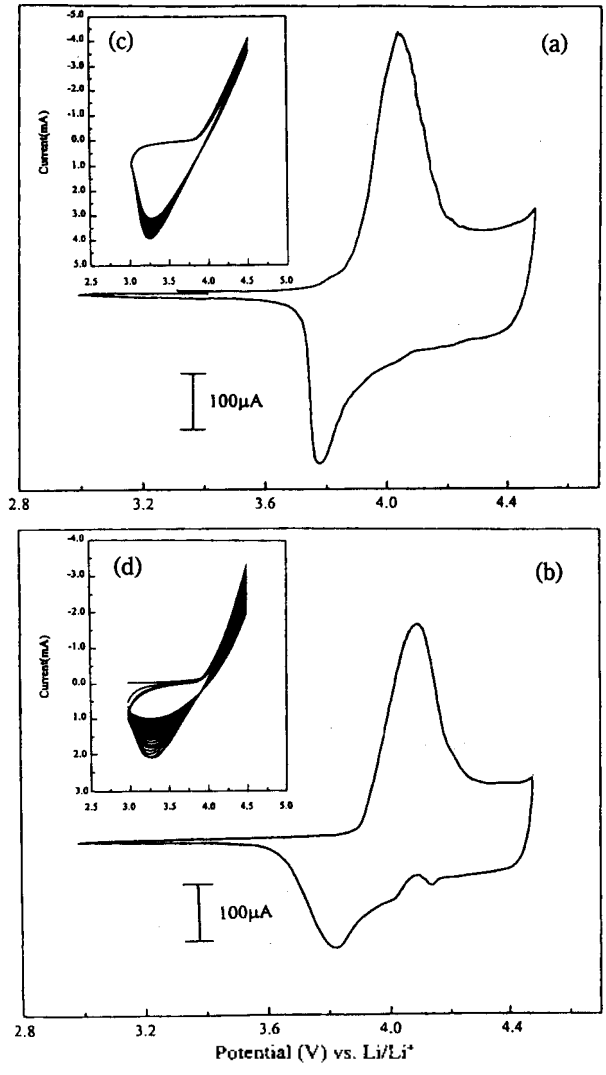

Figure 5. Cyclic voltammograms of (a and c) 600-$LiCoO_2$ and (b and d) 850-$LiCoO_2$ electrodes in 1 M LiClO4/PC. The scan rates were 0.01 mV/sec for (a and b), and 1 mV/sec for (c and d). The potential range was between 3.0 and 4.5 V.

served in the measuring potential range and the reduction peak shifted to the negative direction of 3.25 V in both electrodes. This means that the lithium ions are diffused more slowly into the 850-$LiCoO_2$ crystal structure than the experiment time with the voltages sweep of 1 mV/sec. In recording CVs of about 25 cycles (Figure 5(c)), the magnitude of the oxidation-reduction peaks in the CV recorded for the 600-$LiCoO_2$ electrode reduced slowly, and ultimately the magnitude leveled out and became constant. However, from the largely decreasing reduction peak in the CV recorded for the 850-$LiCoO_2$ electrode (Figure 5(d)), one can expect poor charge-discharge characteristics performance. Thus, the cycleability of the 600-$LiCoO_2$ electrode is better than that for 850-$LiCoO_2$ electrode.

Charge-discharge characteristics of $LiCoO_2$ electrodes. Figure 6(a) shows charge/discharge curves recorded for a 600-$LiCoO_2$/Li cell in the first and second cycles. The cell was first charged at a density of 0.2 mA/cm^2 to an upper limit of 4.4 V. Upon discharging, the lower potential limit was 3.3 V. A plateau in the charge/discharge curve

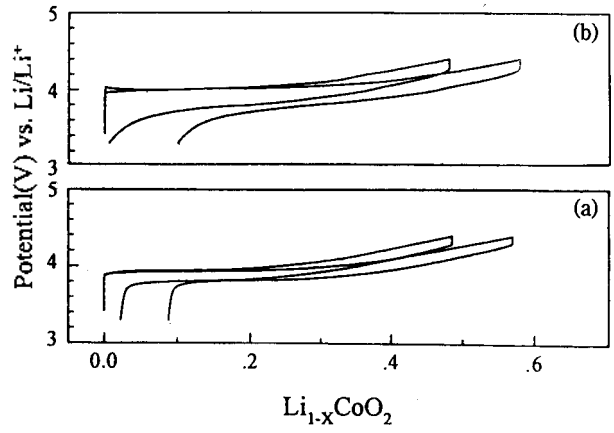

Figure 6. Cell voltages as a function of x in $Li_{1-x}CoO_2$ in the initial charge/discharge step. The charge/discharge range was between 4.4 and 3.3 V with a current density of 0.2 mA/cm^2. (a); 600-$LiCoO_2$ electrode and (b); 800-$LiCoO_2$ electrode.

was observed at about 3.92 V in the 600-$LiCoO_2$/Li cell and the cell potential increased continuously to 4.4 V. A plateau appearing in the curves can be expected from the cyclic voltammetric results shown in Figure 5, which showed a couple of large redox peaks due to the deintercalation/intercalation of lithium ions in the $LiCoO_2$ crystal structure. The charge-discharge curve recorded for the 850-$LiCoO_2$/Li cell shows a large plateau at about 3.98 V and a small distinct plateau associated with a phase transition at 4.18 V (Figure 6(b)). The 600-$LiCoO_2$/Li cell operated in the first charge-discharge capacity at 156-132 mAh/g and the second at 133-127 mAh/g. The 850-$LiCoO_2$/Li cell operated in the first and second charge-discharge capacitys at 158-131 mAh/g and 132-130 mAh/g, respectively. The first charge-discharge capacity is almost the same in both electrodes. During the first charging of the 850-$LiCoO_2$/Li cell, the cell potential increased sharply at about 4.0 V. This phenomenon is due to a high contact resistance of the 850-$LiCoO_2$ electrode, which may originate from the inhomogeneous crystal-particle distribution in the 850-$LiCoO_2$ powder.

Figure 7 shows the cyclability and utilization(%) of 600- and 850-$LiCoO_2$/Li cells, which were charged at a density of 0.5 mA/cm2 in the potential range from 4.2 to 3.6 V. The capacities of the charge-discharge and utilization of the cell were plotted against the cycle number. The initial charge-discharge capacity for the 600-$LiCoO_2$/Li cell was 124-108 mAh/g, and for the 850-$LiCoO_2$/Li cell was 128-109 mAh/g. For the 600-$LiCoO_2$ electrode, the discharge capacity expressed as the Δx value (fraction of Li ions) of $LixCoO_2$ was 0.3 (82.2 mAh/g) in the first cycles and maintained a constant level of about 80 mAh/g over the 25 cycles. However, the value obtained from the 850-$LiCoO_2$/Li cell begin to decrease below Δx=0.3 after the 15th cycle. These behaviors were consistent with the result of the cyclic voltammetric experiment shown in Figure 5. The cathode made by the $LiCoO_2$ powder prepared at the low temperature exhibits more excellent cycling performance than that of the high temperature.

Impedance spectra of $LiCoO_2$ electrode. Figure 8 presents typical impedance spectra in Nyquist presentation

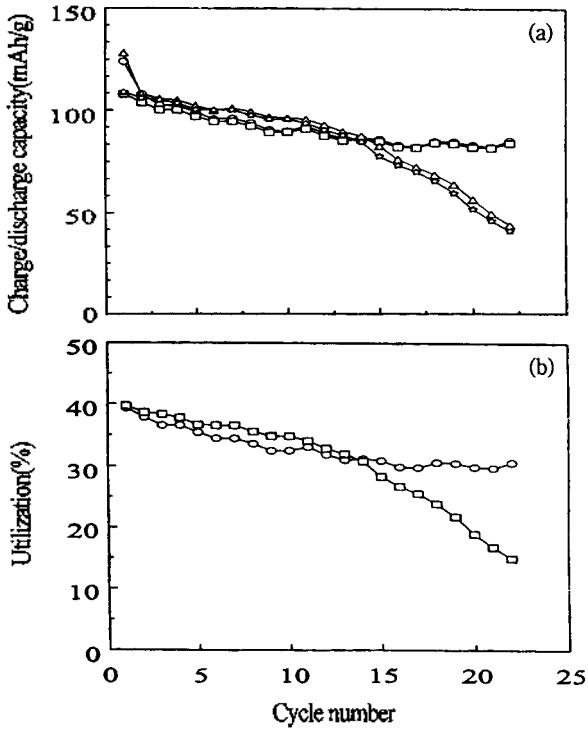

Figure 7. (a) Charge/discharge capacities and (b) utilization variations of the $LiCoO_2$ electrodes according to the cycle number. The cycling potential was between 4.2 and 3.6 V at 0.5 mA/cm^2. (○: the charge capacity of the 600-$LiCoO_2$ electrode, □: the discharge capacity of the 600-$LiCoO_2$ electrode, △: the charge capacity of the 850-$LiCoO_2$ electrode, ☆: the discharge capacity of the 850-$LiCoO_2$ electrode, (b) ○: the utilization of the 600-$LiCoO_2$ electrode, □: the utilization of the 850-$LiCoO_2$ electrode.

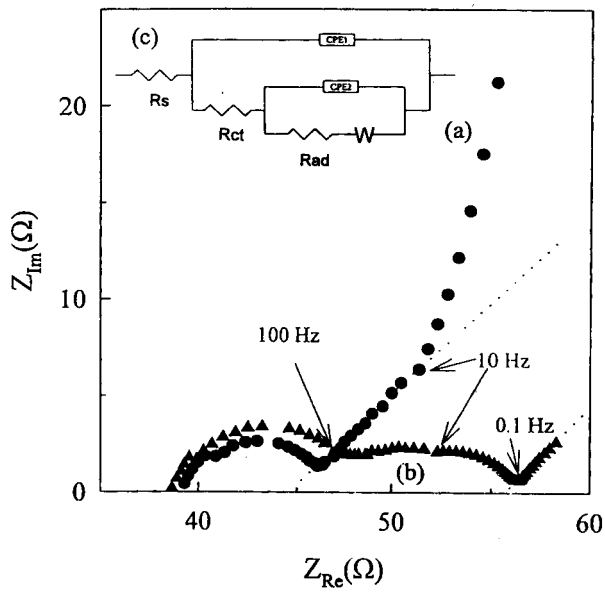

Figure 8. Impedance spectra recorded for the 600-$LiCoO_2$/Li cell at (a) x=0 and (b) x=0.51 in $Li_{1-x}CoO_2$, and (c) an equivalent circuit for the spectra. The pulse amplitude was 5 mV and the measuring frequency was between 100 kHz and 5 mHz.

for the 600-$LiCoO_2$ electrode and its equivalent circuit. They were recorded between 100 kHz and 5 mHz with a pulse amplitude of 5 mV. Figure 8(a) shows a spectrum recorded at x=0 in $Li_{1-x}CoO_2$, which has an arc at a frequency range of 100 kHz-100 Hz, a line inclined at about 45° to the real axis between 100-10 Hz arising from the diffusion of lithium ions through the $LiCoO_2$ crystal structure, and another line associated with a capacity term in a frequency range below 10 Hz. Figure 8(b) shows a spectrum recorded at x=0.51, which has two separated arcs over the high and intermediate frequency ranges and a line inclined to the real axis. The first arc in the high frequency range above 100 Hz is due to the charge transfer reaction at the interface of the electrolyte/electrode interface. The second arc in the middle frequency range between 100 Hz and 100 mHz is from the impedance due to the adsorbed layer with an excess of lithium ions which exist near the surface region of the oxide electrode. The inclined line at about 45° to the real axis in the range below 100 mHz is from the Warburg impedance term associated with the diffusion of lithium ions within the $LiCoO_2$ electrode.[16] The equivalent circuit was derived from "Equivalent Circuit" program distributed through EG&G PAR by Universiteit Twente.

Table 1 shows the changes of the charge transfer resistance, Rct, at the electrode and electrolyte interface and of the resistance due to the adsorbed layer, Rad, formed onto the electrode surface by the constant current charging.[16] The values of the charge transfer resistance remain nearly constant irrespective of the amounts of lithium ions, since the charge transfer reaction occurs in the $LiCoO_2$.[17] The value of the diffusion coefficient D_{Li}^+ in the $LiCoO_2$ electrode was calculated from the following equation:[24]

Table 1. Values for the parameters obtained from Impedance spectra of the 600-$LiCoO_2$ electrode

Charging capacity, mAh/g	R_s, Ω	R_{ct}, Ω	Q_1		R_{ad}, Ω	Q_2		Q_3 (W)		χ^2, $\times 10^{-4}$
			$Y_{0,1}$ mho $\times 10^{-5}$	n_1		$Y_{0,2}$ mho $\times 10^{-3}$	n_2	$Y_{0,3}$ mho $\times 10^{-3}$	n_3	
OCV	38.2	8.44	9.61	0.704	-	2.43	-	5.56	-	
20	38.8	6.01	1.95	0.906	9.13	4.64	0.705	1.33	0.584	2.05
40	38.6	6.67	2.40	0.888	7.19	3.63	0.740	1.58	0.567	2.22
60	38.6	7.71	4.76	0.810	6.80	4.13	0.743	1.90	0.571	2.71
80	38.6	7.71	3.26	0.847	7.52	4.99	0.689	1.95	0.561	2.60
100	38.6	7.88	2.32	0.882	8.40	5.76	0.653	2.44	0.569	1.92
120	38.5	7.90	2.03	0.896	9.07	6.69	0.614	2.45	0.574	1.83
140	38.6	8.10	2.18	0.890	9.80	7.61	0.589	3.16	0.653	1.82
170	39.4	8.10	2.20	0.893	9.67	7.17	0.569	2.46	0.721	1.72
190	39.5	7.79	2.51	0.885	8.79	7.54	0.562	1.89	0.699	1.51

$$D_{Li} = \frac{\pi f_T r^2}{1.94}$$

where f_T is the frequency at the transition from the semi-infinite diffusion behavior to finite-length diffusion behavior and r is the average radius of the $LiCoO_2$ particles. In the case of (a) in Figure 8, the chemical diffusion coefficient D_{Li}^+ was 4.6×10^{-8} cm^2/sec. It is observed that for (b) the chemical diffusion coefficient D_{Li}^+ is lower by about three orders. After the deintercalation of lithium ions, a similar impedance spectrum was observed in all ranges. It is thought that its relative low diffusivity is due to the repulsive force between the oxygen atoms in the more disordered structure of the 600-$LiCoO_2$ powder.

Conclusions

In this study, the precursor of $LiCoO_2$ powders was synthesized by a sol-gel method in an aqueous solution containing LiOH and $Co(OAc)_2$. $LiCoO_2$ powders were prepared from heat-treatments of the precursor at 600 °C and 850 °C. The 600-$LiCoO_2$ powder has a homogeneous particle size of about 1 μm and its crystal structure is consistent with the previous reported crystal structure,[18] while the 850-$LiCoO_2$ had a widely distributed particle size of 10-25 μm. Upon charging and discharging with a current density of 0.2 mA/cm^2 in a potential range from 4.4 to 3.3 V, the initial charge-discharge capacities of 600- and 850-$LiCoO_2$/Li cells were 156-132 mAh/g and 158-131 mAh/g, respectively. The discharge capacity of the 600-$LiCoO_2$/Li cell did not decrease below Δx=0.3 (82.2 mAh/g) and maintained a constant level after 25th cycles. However, the discharge capacity of the 850-$LiCoO_2$/Li cell dropped below Δx=0.3 after the 15th cycle at a density of 0.5 mA/cm^2 in the potential range of 4.2-3.6 V. The diffusion coefficient D_{Li}^+ was 4.6×10^{-8} cm^2/sec, calculated from the impedance measurements for the 600-$LiCoO_2$ electrode.

Acknowledgment. This work was supported by Korea Science and Engineering Foundation (the project number: 961-0304-030-2).

References

1. Brandt, K. *Solid State Ionics* **1994,** *69*, 173.
2. Mithusima, K.; Jones, P. C.; Wiseman, P. J.; Goodnough, J. B. *Mat. Res. Bull.* **1980,** *15*, 783.
3. Plichta, E.; Slane, S.; Uchiyama, M.; Salmon, M. *J. Electrochem. Soc.* **1989,** *136*, 1865.
4. Reimers, J. N.; Dahn, J. R. *J. Electrochem. Soc.* **1992,** *139*, 2091.
5. Gummow, R. J.; Thackeray, M. M. *Mat. Res. Bull.* **1992,** *27*, 327.
6. Ohzuku, T.; Ueda, A. *J. Electrochem. Soc.* **1994,** *141*, 2972.
7. Amatucci, G. G.; Tarascon, J. M.; Klein, L. C. *J. Electrochem. Soc.* **1996,** *143*, 1114.
8. Ohzuku, T.; Ueda, A.; Nagayama, M. *J. Electrochem. Soc.* **1993,** *140*, 1862.
9. Ebner, W.; Fouchard, D.; Xie, L. *Solid State Ionics* **1994,** *69*, 238.
10. Ueda, A.; Ohzuku, T. *J. Electrochem. Soc.* **1994,** *141*, 2010.
11. Inaba, M.; Todzuka, Y. *Chemistry Letters* **1995**, 889
12. Bach, S.; Henry, M.; Baffier, N.; Livage, J. *J. Solid State Chem.* **1990,** *88*, 325.
13. Guyomard, D.; Tarascon, J. M. *J. Electrochem. Soc.* **1992,** *139*, 937.
14. Manev, V.; Banov, B. *J. Power Sources* **1995,** *57*, 99.
15. Yoshio, M.; Tanaka, H.; Tominaga, K.; Noguchi, H. *J. Power Sources* **1992,** *40*, 347.
16. Jeong, E. D.; Shim, Y.-B. *J. Power Sources* **1997**, in press.
17. Choi, Y.-M.; Pyun, S.-I.; Moon, S.-I. *Solid State Ionics* **1996,** *89*, 43.
18. Barboux, P.; Tarascon, J. M.; Shokoohi, F. K. *J. Solid State Chem.* **1991,** *94*, 185.
19. Chang, H. S. W.; Lee, T. T.; Lin, S. C.; Jeng, J. H. *J. Power Sources* **1995,** *54*, 403.
20. Garcia, B.; Farcy, J.; Pereira-Ramos, J. P.; Perichon, J.; Baffier, N. *J. Power Sources* **1995,** *54*, 373.
21. Hwang, H.; Bruce, P. G. *J. Electrochem. Soc.* **1994,** *141*, L106.
22. Bach, S.; Henry, M.; Barrier, N.; Civage, J. *Solid State Chem.* **1990,** *88*, 325.
23. Nakamoto, K. In *Infrared & Raman spectra of inorganic and Coordination Compounds*; John Wieley & Sons: 1986; p 139.
24. Cabanel, R.; Barral, G.; Diard, J. P.; Le Gorrec, B.; Montella, C. *J. Appl. Electrochem.* **1993,** *23*, 93.